NDT&E International 62 (2014) 66–76

Contents lists available at ScienceDirect

NDT&E International

journal homepage: www.elsevier.com/locate/ndteint

Crack detection limits in unit based masonry with terrestrial laser scanning

Debra F. Laefer [a,*], Linh Truong-Hong [b], Hamish Carr [c], Manmeet Singh [d]

[a] School of Civil, Structural and Environmental Engineering (SCSEE) and Lead PI, Urban Modelling Group (UMG), University College Dublin (UCD), Newstead G25, Belfield, Dublin 4, Ireland
[b] SCSEE and UMG, Newstead G27, Belfield, Dublin 4, Ireland
[c] School of Computing, Faculty of Engineering, University of Leeds, EC Stoner Building 9.25, Leeds, UK
[d] SCSEE and UMG, UCD, Newstead G67, Belfield, Dublin 4, Ireland

ARTICLE INFO

Article history:
Received 15 May 2013
Received in revised form
16 October 2013
Accepted 8 November 2013
Available online 21 November 2013

Keywords:
Terrestrial laser scanning
Point cloud data
Crack detection
Structural health monitoring
Condition assessment
Masonry

ABSTRACT

This paper presents the fundamental mathematics to determine the minimum crack width detectable with a terrestrial laser scanner in unit-based masonry. Orthogonal offset, interval scan angle, crack orientation, and crack depth are the main parameters. The theoretical work is benchmarked against laboratory tests using 4 samples with predesigned crack widths of 1–7 mm scanned at orthogonal distances of 5.0–12.5 m and at angles of 0°–30°. Results showed that absolute errors of crack width were mostly less than 1.37 mm when the orthogonal distance varied 5.0–7.5 m but significantly increased for greater distances. The orthogonal distance had a disproportionately negative effect compared to the scan angle.

© 2013 Elsevier Ltd. All rights reserved.

1. Introduction

Surface crack identification and maximum crack width determination have long played important roles for condition and risk assessment of buildings (e.g. [1,2]). To this end, several instruments have been developed to either detect visible cracks or measure crack characteristics (e.g. length and width). Mechanical probes and electronic sensors are generally used [3–5]. However, while such instruments offer high precision for crack measurement, most have significant limitations: (1) predefined permanent positions on the structure; (2) prefixed, uniaxial measurement; (3) limited measurement range; (4) physical access requirements, and/or (5) considerable cost. To overcome these shortcomings, there has been a great interest in non-contact, image-based methods including photogrammetry and terrestrial laser scanning (TLS) to measure structural deformations [6–8], detect surface decay [9], and estimate mass loss [6,10]. In such cases, as well as in crack detection, most published research only presents empirical limits. The following study provides a mathematical basis for using TLS to detect cracking in unit-block masonry (i.e. stone, brick, or concrete masonry units).

2. Related work

Photogrammetry and laser scanning are often adopted to overcome the five limitations listed above. Since a fairly systematic overview of the wider range of techniques applicable to cultural heritage and civil infrastructure was recently published elsewhere (e.g. [11]), this background section is restricted to image- and laser scanning-based methods for structural deformation, mass and volume loss, and defect detection.

In image-based methods, digital images provide geometric and radiometric content to measure the crack width and boundaries. Image-based crack detection has some definitive advantages as it (1) generates a permanent record, (2) is repeatable, (3) circumvents direct contact, and (4) enables crack-by-crack analysis. The last is an advantage over many other approaches such as acoustic emissions where only the severity and density of cracking can easily be ascertained [12]. Barazzetti and Scaioni [13] employed the RGB intensity component to extract the sides of a crack in a wide variety of construction materials (e.g. concrete, brick, and asphalt) and then computed the crack width at a given cross-section. When compared to results from mechanical probes and

* Corresponding author. Tel.: +353 17163226; fax: +353 17163297.
E-mail addresses: debra.laefer@ucd.ie (D.F. Laefer), linh.truonghong@ucd.ie (L. Truong-Hong), h.carr@leeds.ac.uk (H. Carr), manmeet.singh@ucdconnect.ie (M. Singh).

0963-8695/$ - see front matter © 2013 Elsevier Ltd. All rights reserved.
http://dx.doi.org/10.1016/j.ndteint.2013.11.001

electronic sensors, the proposed procedure reported crack measurement errors in the range of ±5 μm to ±19 μm. In contrast, Hampel and Maas [14] applied a cascade image analysis approach to estimate crack width in textile-reinforced concrete in tension testing. In this approach, edge detection techniques were applied to dense displacement vector fields generated by image matching techniques obtained from consecutive images. That study reported that hairline cracks 1/20 of a pixel wide could be detected at a precision of 1/50 of a pixel, but that errors of crack position were 5.8 pixel in each coordinate direction. Additionally, Niemeier et al. [15] implemented the polyline-fly-fisher algorithm proposed by Dare et al. [16] to estimate outliers and to determine the mean crack width from images taken by a digital retinal scanner camera. The approach required users to choose start and end points of the crack. Six field tests showed a relative error in measuring crack width of approximately 15%, while the largest absolute error was 0.05 mm for a 3 mm wide crack.

To monitor crack changes in concrete surfaces, Sohn et al. [17] modified a Hough transform based algorithm (as previously proposed by Habid and Kelley [18]) to estimate 2D transformation parameters for registering sequential images, while the crack itself was extracted using image-processing techniques (e.g. enhancement, noise removal, histogram thresholding, thinning). Object coordinates in subsequent images were analyzed to determine any changes. The error in calculating the object coordinates of the crack was ±0.3 mm. While image-based methods can provide good accuracy, they require supplementary information that is not always readily available, such as camera lens, focal length, or the exact distance from the camera to the target surface. As an alternative, interest in terrestrial laser scanning has rapidly increased.

However, to date, most research using laser scanners in structural assessment has focused on measuring structural deformation, estimating material loss, or finding surface defects. For structural deformation, Gordon et al. [8] compared vertical displacements from the LMS-Z210 and Cyrax 2500 TLS units against photogrammetry. The root mean square (RMS) of the differences was in the range of ±2.4 mm to ±9.5 mm for the LMS-Z210 and as little as ±0.29 mm for the Cyrax 2500 TLS. To detect bowing of marble cladding, Al-Neshawy et al. [19] used the FARO LS 880HE80 scanner to achieve a sampling step of approximately 1 mm at a distance of 4.36 m, in which the semantic distance error was ±3 mm. The TLS based results showed the magnitudes to differ 1–2 mm for convex bowing and 6–7 mm for concave ones when compared to manual measurements, in which the bowing magnitude was expressed as a term of the measured value of bowing over the distance between the supports of the 950 mm long marble panel. Olsen et al. [6] detected structural damage of reinforced concrete beam-columns using TLS. Volumetric calculations were performed using the crossing section method. In that, the specimen was divided into multiple sections, and then the volume was calculated based on the area of a polygon by fitting data points on a section and the thickness between two consecutive sections. Volume loss was recognized by comparing the determined volumetric surface to that of the original structure.

Concrete surface mass loss was automatically recognized in TLS data based on the analysis of curvature distributions in equally sized sub-areas divided within a scanning region [10]. The principal curvatures were computed by using methods of differential geometry. Damage was detected when the Gaussian curvature distribution changed dramatically in a sub-area. The method failed, when data noise exceeded 0.8–1.0 cm, or if a crack had a width significantly lower than the linear dimension of the sub-area. For detecting changes in excavation volume, Girardeau-Montaut et al. [20] looked at two approaches using octree-based comparisons. In one, a pair of sub-sets of points was contained in two homologous cells of the source, and target clouds were compared based on the average distance from a best plane fitting. In the other, the Hausdorff distance was used to identify changes over time. The latter was reported as more precise but slower; however quantification of the results was not given.

Armesto-González et al. [9] used an automated classification algorithm to analyze 2D intensity images generated from 3D point clouds for detection of moisture based damage in historic stone buildings. This work used various TLS units (e.g. FARO Photon, TRIMBLE GX200, and RIEGL-Z390i) to collect data. Damaged ashlars with differing moisture contents were reported. In concrete, Liu et al. [21] proposed distance and gradient based criteria for detecting defective areas of the extended pile cap of a concrete bridge. For this work, the reference plane was defined, and a selected area for analysis was divided into smaller grids, in which a data point was arranged with column and row numbers. Then, gradient and distance information in the reference plane were calculated. The grid area was considered to contain a defect, if the gradient and distance were larger than predefined thresholds; no guidance was provided for threshold selection. In an alternative approach, to identify cracks in asphalt paving, Tsai and Li [22] used a dynamic-optimization-based crack segmentation method followed by a linear-buffered Hausdorff scoring method for quantitative crack segmentation.

So while TLS has been used successfully for measuring structural deformation and monitoring surface deterioration, crack identification and documentation still remains a challenge because of an absence of a rigorous, mathematically based methodology from which inspection programs can be devised. The first step to

Table 1
Summary of technical specifications of commercial scanning system.

Brand	ThirdTech [25]	FARO [26]	Trimble [27]	Optech incorporated [28]	Leica geosystems [29]	RIEGL laser [30]
System	DeltaSphere-3000IR	Focus 3D	FX	ILRIS-HD	Leica ScanStation C10	RIEGL VZ-6000
Metrology method	Phase	Phase	Phase	Pulse	Pulse	Pulse
Min./max. range (m)	0.3/16	0.6/120	2/350	3.0/1200	0.1/300	5/6000
Point accuracy* (1 sigma)	5 mm	2 mm @ 10 m and 25 m	0.4 mm @ 11 m; 0.8 mm @ 21m; 2 mm @ 50 m	3–4 mm @ 100 m	6 mm @ 1–50 m	15 mm @ 150 m
Beam diameter	7 mm @ 9 m	3 mm	2.3 mm @ 5 m; 16 mm @ 46 m	19 mm @ 100 m	4.5 mm @ from 0 to 50 m (FWHH-based)	15 mm @ exit; 60 mm @ 500 m
Scan angle step size H/V (°)	0.015/0.015	0.009/0.009	0.01/0.005	0.000745	Minimum point spacing < 1 mm	0.002–3/0.002–0.280
Scan angle accuracy H/V (°) (1 sigma)	0.015/0.015	0.015	0.008	0.046	0.003	0.0005
Field of view H/V (°)	360/290	360/305	360/270	40/40	360/270	360/60

* Positional measurement.

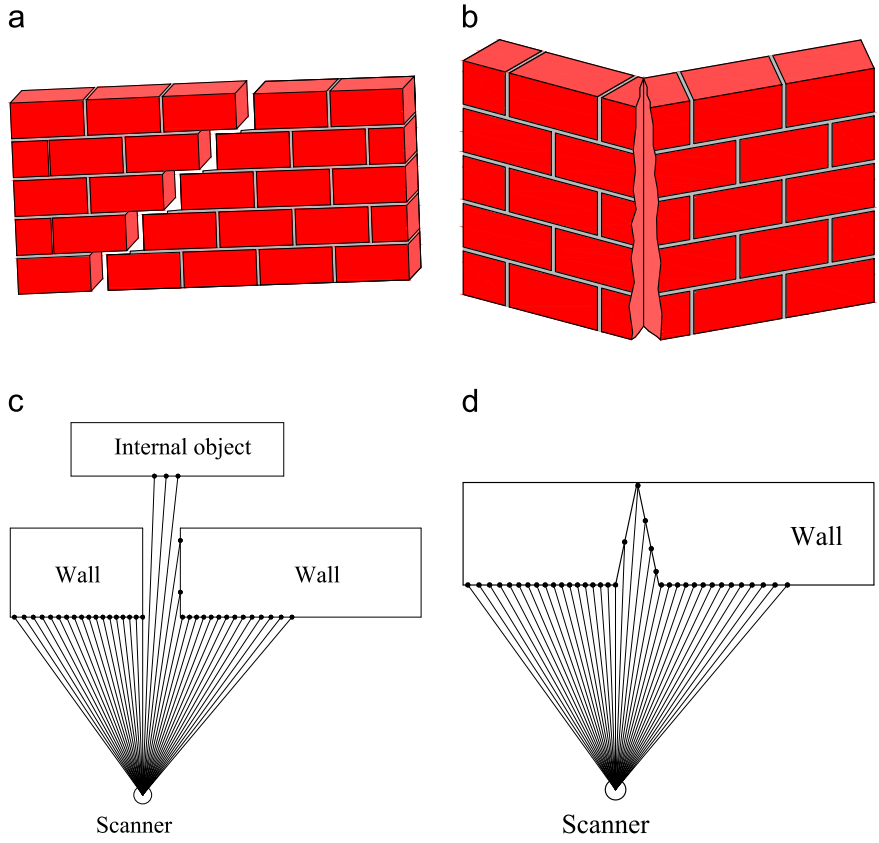

Fig. 1. Common crack shapes in masonry walls. (a) Fully opened crack. (b) Partially opened crack. (c) Scanning process with fully opened crack. (d) Scanning process with partially opened crack.

overcoming this deficit is to understand the range and capabilities of current hardware as presented through a survey of common terrestrial units in the next section.

3. Equipment

Laser scanners measure an object's surfaces based on the elapsed time between signal transmission and reception. In general, there are two types: phase-based and pulse-based (time of flight) scanners. With phase-based scanners, the time delay is measured by the phase difference between the sent and received waveforms. With pulse-based scanners, the time delay is based on the light traveling from the transmitter to the target, plus the time of the reflective light traveling back to the detector. Table 1 provides abbreviated technical specifications for a sampling of popular scanners involving measured range, accuracy, beam diameter, sampling step, and maximum scan angle. Phase-shift systems are best suited for short-range tasks (0.3–350 m) and acquire data points with a nominal accuracy of 0.4 mm for a measurement range of 11 m. Pulse systems are better suited for long-range scanning (up to 6000 m), and the accuracy in terms of point measurement can reach 4 mm for a measurement range of 150 m. Additionally, point accuracy is typically expressed in Cartesian coordinates (x, y, and z), as a function of the measurement range (e.g. an accuracy of 0.8 mm at the measurement range of 21 m). The beam diameter is the diameter along any specified line that is perpendicular to the beam axis and intersects it. This parameter can cause positional uncertainty [23]. Moreover, the scan angle step, which is the ability to resolve two equally intense point sources on adjacent lines of sight, is a function of the spatial sampling interval and the laser beam diameter. With a specific scan distance, the footprint of the beam width on the object may be greater than the sampling step, which causes overlapping laser spots. To obtain sufficient spatial resolution for estimating the level of details from the TLS data, Lichti and Jamtsho [23] suggested that the sampling interval be set equal to the beam width. However, through a study of the influence of the scan angle step in distinguishing adjacent elements, Pesci et al. [24] identified that adjacent elements can be recognized once the gap is greater than a third of the laser beam. The minimum incremental angles in the phase-shift and pulse systems are, respectively, 0.005° and 0.000745°. In TLS, a rotating optical device is used in a transmitting laser beam to an object and receiving the return beam; the two angles are theoretically the same. The accuracy angle is used to measure the difference between the two angles through a mechanical axis or other optical rotating device. The largest angular error is 0.046° for the ILRIS-HD scanner. Finally, the field of view offers possible angle scanning ranges in the horizontal and vertical directions.

4. Geometric basis for limitations on crack detection

In masonry structures (i.e. stone, brick, or concrete masonry units), cracks often run through the head and/or bed joints and are usually either vertical or horizontal. This simplifies detection, however a crack may or may not be fully separated, which complicates the mathematics (Fig. 1a vs. b). In the fully open case, when the horizontal angle is small, the laser beam may reflect objects from behind the wall (Fig. 1c). In the partially open case, the laser beam may touch either the back or the side faces of the

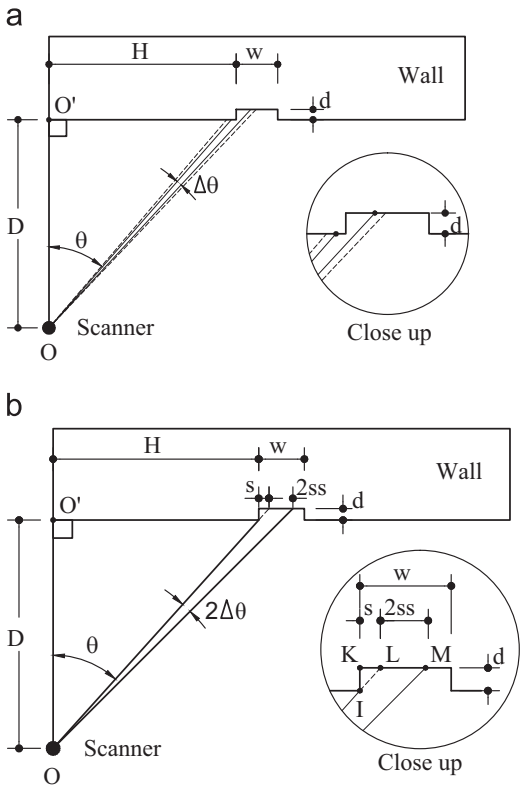

Fig. 2. Schematic diagram of a wall crack and laser scanner. (a) Assumed crack shape (plan view). (b) Diagram for predicting a minimum crack width (plan view).

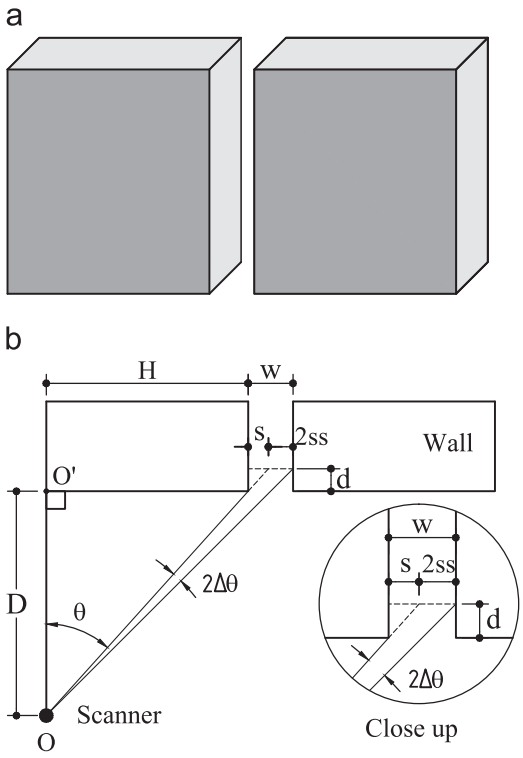

Fig. 3. Schematic diagram of a fully open crack and its relation to a laser scanner's beam. (a) Elevation and (b) A cross-section.

crack (Fig. 1d). Irrespective of the case, point data within the crack lie on a plane distinctive from that of the wall.

During point cloud data collection of a wall, two parameters impact the quantity and quality of the data: the distance between the scanner (D) and the offset angle (θ). The crack can be recognized based on the distance from the crack plane to the wall, which is called the crack depth (d) (Fig. 2). Thus, crack detectability depends on D, θ, and d. To develop the mathematical formula to determine the narrowest crack detectable by a TLS unit, three assumptions are made about the crack: (1) it is vertical; (2) it has a consistent rectangular cross-section with a finite depth that is equivalent to a non-fully separated crack (Fig. 2a and 3); it is located at the same elevation as the scanner. More complicated cases will be presented subsequently.

While a crack edge can lie in the space between two consecutive laser beams (Fig. 2a), the ideal case for establishing the minimum detectable crack width is when the laser beam touches the crack edge closest to the scanner (Fig. 2b). In that case, the scanner reflects from the back face of the crack. The shadow region (as represented by the triangle IKL in the close up of Fig. 2b) with its width (s) is created, in which there are no data points (Fig. 2). When a laser scan beam spreads across a surface containing a crack, the returning data points may lie on multiple surfaces (forward surface and back of crack). With very small horizontal incremental angle steps and crack depths, it is hard to distinguish between two consecutive sample points, in which one belongs to the object's exterior surface and the other to the back of the crack. To determine the minimum visible crack, there must be at least two reflected laser beams returning from the back face of the crack (Fig. 2b), corresponding to twice the horizontal sampling step ($2ss$) or the segment length LM (Fig. 2b). Since the sampling step s is proportional to the scan angle and the range (i.e. distance) to the object [31,32], the minimum visible crack can be expressed by Eq. (1):

$$w \geq s + 2ss \tag{1}$$

where s is the shadow width (Fig. 2), and ss is the horizontal sampling step with the interval scan angle $\Delta\theta$. Because the triangle OO'I (Fig. 2b) is similar to the triangle IKL, the angle $\angle$KIL equals the scan angle θ. The shadow width is given as Eq. (2).

$$s = d \tan \theta \tag{2}$$

Based on the assumption of multiple laser beams hitting the back face of the crack, the point M is the vertex of a triangle with an angle at the scanner of $\theta + 2\Delta\theta$ (Fig. 2b). Applying the tangent rule to this angle, O'OM (Fig. 2) results in Eq. (3):

$$\tan(\theta + 2\Delta\theta) = \frac{H + s + 2ss}{D + d} \tag{3}$$

where D is the orthogonal distance from the scanner to the object, and H is the distance from the scanner to the closest crack's edge in the horizontal direction. By manipulating Eq. (3), the minimum crack width can be expressed as Eq. (4):

$$s + 2ss = (D + d) \tan(\theta + 2\Delta\theta) - H \tag{4}$$

Substituting the inequality in Eq. (2) into Eq. (4), the minimum crack width can be expressed as Eq. (5):

$$w \geq (D + d) \tan(\theta + 2\Delta\theta) - H \tag{5}$$

Therefore, the minimum crack width depends on the angle step of the scanner, the relative location between the scanner and the crack, and the crack depth. Interestingly, Eq. (5) can be also used to determine a crack width of a fully open crack (Fig. 1a and Fig. 3a and b). In this case, the crack width can be calculated from Eq. (1) and is equal to the term on the right side of Eq. (5) (see case Fig. 3b). As angle $2\Delta\theta$ is very small, the tangent of the angle $(\theta + 2\Delta\theta)$ is approximately equal to the tangent of the angle (θ).

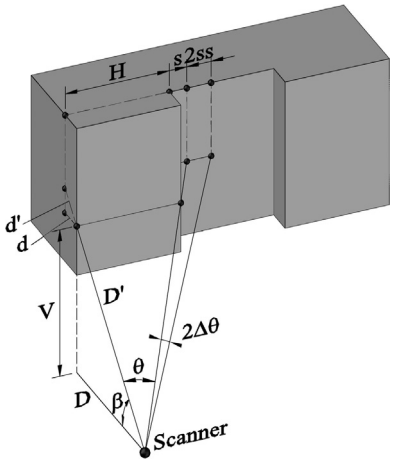

Fig. 4. Diagram of laser beams and crack different level from the scanner's mount.

As such, the crack depth can be determined with Eq. (6):

$$d = \frac{w}{\tan\ \theta} \tag{6}$$

In addition, the minimum detectable crack width of a horizontal crack can be predicted by using Eq. (5), by defining $\Delta\theta$ as the vertical scan angle step. However, in practice, the crack elevation commonly differs from that of the scanner's mount. If the crack is offset vertically by V, and the horizontal distance between the scanner to the closest crack edge remains H, then Eq. (5) can be used, where variables D and d are replaced by D' and d', respectively (Fig. 4). Of which, D' is the distance from the scanner's mount to the wall at vertical scan angle of β, while d' is the distance from the front wall to the back face of the crack along direction of a laser beam (Fig. 4). From the schematic diagram in Fig. 4, D' and d' can be expressed as Eqs. (7) and (8):

$$D' = \sqrt{D^2 + V^2} \tag{7}$$

$$d' = d\ \cos\ \beta \tag{8}$$

$$\beta = a\ \tan\left(\frac{V}{D}\right) \tag{9}$$

$$\theta = a\ \tan\left(\frac{D'}{H}\right) \tag{10}$$

As such, the crack width of a vertical crack located at a different level from the scanner's mount can be expressed by Eq. (11):

$$w \geq (D' + d')\ \tan\ (\theta + 2\Delta\theta) - H \tag{11}$$

Unfortunately, consistent usage of TLS data for crack detection is not trivial, because the quality and density of a point cloud depends on the scanner, environment, target surface, and location of the scanner with respect to the target. Herein, establishing the accuracy of crack width-based data, an ideal scenario is assumed, in which the data points are distributed regularly at a grid spacing proportional to the measurement range and scan angle step (Fig. 5a) and with no noise within the data. As part of the subsequent experimental verification presented herein, the differences between the ideal, crack width-based point cloud and the actual one were obtained.

The TLS unit operates in a spherical coordinate system, with regular horizontal and vertical incremental angles, in which the

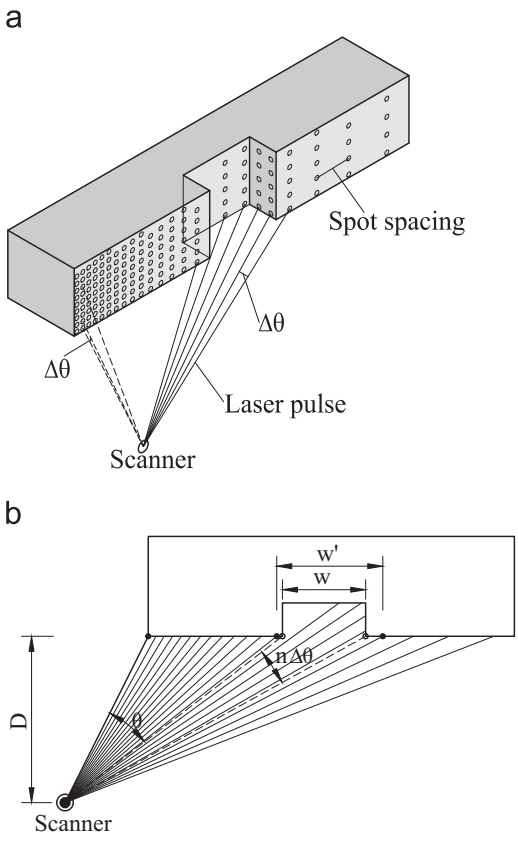

Fig. 5. Scan mechanism of crack detection by TLS. (a) Ideal three-dimensional scanning mechanism. (b) Ideal two-dimensional scanning mechanism.

scanner is at the origin. Data points on the object's surface lie in a different plane from ones of the back face of the crack (Fig. 5). Therefore, after eliminating data points from the back face of the crack, the crack width can be determined as the distance between a pair of sample points located to the left and right of the crack's edges (Fig. 5b).

Because the output of the laser beam was treated as a point or set of points on a surface, if $n+1$ points are detectable in the crack, there are n spaces. Based on the assumption that the laser beam touches the crack's two edges (dashed lines in Fig. 5b), the crack width can be given as Eq. (12):

$$w = D[\tan(\theta + n\Delta\theta) - \tan\ \theta] \tag{12}$$

where n is the number of spaces in the crack width.

Solving Eq. (11), the number of scan beams can be expressed as Eq. (13):

$$n = \frac{a\ \tan(w/D + \tan\ \theta) - \theta}{\Delta\theta} \tag{13}$$

However, as TLS data collection is discrete, there is no guarantee that the returned points are on the crack's edge and not outside (e.g. the two bold continuous lines in Fig. 5b, as opposed to the dashed ones). Therefore, the actual number of the spaces over the crack width is equal to n', where n' is rounded up to the nearest integer of n solved from Eq. (13). Consequently, the measured crack width, w', can be calculated by Eq. (12) by using the values of n' instead of n. Error propagation analysis of measured crack width due to positional uncertainty of a point cloud can refer Appendix A.

5. Verification

To verify the above equations, laboratory tests were conducted for various vertical cracks at different locations from the scanner. The goal was to determine a minimum detectable crack at a range of positions, with respect to the scanner. This is based on the hypothesis that for a given scanner there should be an essentially linear relationship between offset and crack detection. In this case, a Trimble GS200 3D scanner (technical specifications summarized in Table 2) was used to collect point clouds of the samples [33]. Subsequently, crack widths were determined manually by an experienced operator using the RealWorks Survey (RWS) V6.3 software associated with the Trimble scanner [34].

The model, vertical crack was created by mounting pairs of cast concrete blocks (25 mm wide $\times$ 25 mm depth $\times$ 145 mm long), at a uniform distance from each other on a wooden board (Fig. 6a). The samples had intended separations of 1 mm, 3 mm, 5 mm, and 7 mm for samples S1–S4, respectively. Actual crack widths were respectively 1.10 mm (Standard deviation [std]=0.05 mm), 3.14 mm (std=0.15 mm), 5.33 mm (std=0.12 mm) and 7.27 mm (std=0.09 mm), as measured by electronic callipers with an accuracy of 0.01 mm (Fig. 6b). Each sample was scanned at orthogonal distances (D) from the scanner 5 m–12.5 m at 2.5 m intervals and scan angles (θ) of 0°, 15°, and 30° (Fig. 6c). The sample S4 was only scanned at 30°. During data acquisition, the smallest sampling step was set at 3 mm, at a measurement range of 100 m. The scanner head was placed at the same elevation as the vertical centre of the samples.

Table 2
Summary technical specifications of the Trimble GS200.

Aspects	Technical parameters
Metrology method	Time of flight
Range measurement	2–200 (m)
Point accuracy	1.4 mm at 5–50 m
Beam diameter	3 mm at 50 m
Minimum sampling step	3 mm at 100 m
Angular accuracy (horizontal/vertical)	0.0018°/0.0009°
Field of horizontal/vertical view	360°/60°

Quality of TLS data depends on various parameters: (i) the scanner mechanism, (ii) atmospheric and environmental conditions, (iii) object properties, and (iv) the scanning geometry [32]. Post-processing data in geometric computation based data points is often affected by the quality of all data points of interest. The noise level of a data set of the sample surface (excluding points of crack's faces) in this study was computed similarly to the proposal by Soudarissanane et al. [32] based on a incidence angle and a normal vector of the fitting surface reconstructed from data points of interest. At each location of each sample, the point cloud on the sample's surface was extracted by using a built-in segmentation tool in RWS V6.3. The noise level in the direction of the laser beam, the perpendicular of the fitting surface, and the standard errors of these noise level (σ) are given in Eqs. (14)–(16), respectively:

$$e_\rho = P_M N^T \tag{14}$$

$$e_d = e_\rho \cos \alpha \tag{15}$$

$$\sigma = \sqrt{\frac{ee^T}{n}} \tag{16}$$

where P_M is the mean deviated points of the given data set involving n points, N is the normal vector of the fitting plane estimated by using a least square method, α is the incidence angle, which is an angle between the normal vector of the fitting surface and the laser beam, and e is applicable to both Eqs. (14) and (15), respectively, when applied individually.

The results of the standard errors of these noise levels are shown in Table 3. The values were varied in each sample, with a scan distance and angle. The averages of the standard error of the perpendicular noise level are 2.01 mm, 2.20 mm, 2.16 mm and 1.76 mm for samples S1–S4, respectively.

To measure the crack widths, the point cloud of each sample was registered in RWS V6.3 and extraction of data points of a sample's surface and measurement of crack width were conducted within RWS V6.3 (Fig. 7). As shown in Fig. 7a, the data point of the sample surface including the crack's face (defined with a rectangle shown within the dashed lines) was manually segmented by using a built-in segmentation tool in RWS V6.3, where points outside of the rectangle were eliminated based on the premise that they

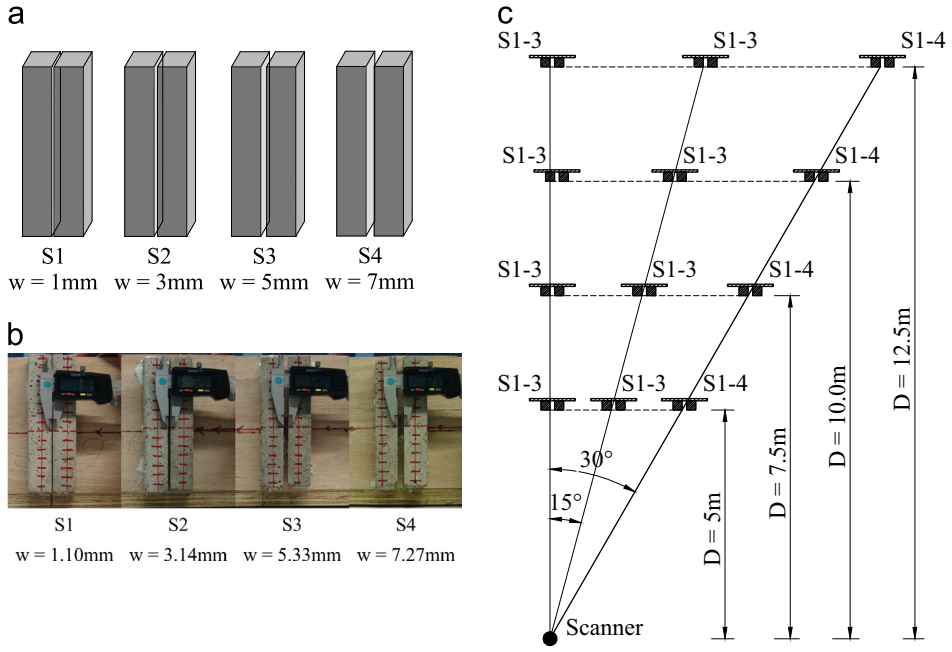

Fig. 6. Verification tests. (a) Four samples. (b) Crack widths after the actual samples. (c) Plan of laboratory tests.

Table 3
Standard errors of the noise level.

Scan angle	$D=5.0$ m Crack width (mm)				$D=7.5$ m Crack width (mm)			
	1	3	5	7	1	3	5	7
0.0	1.9278* (2.2626)+	1.9837 (1.995)	1.9414 (1.9451)		1.8773 (2.5859)	1.9343 (2.5549)	1.7153 (2.4241)	
15.0		2.2072 (2.2745)	1.8829 (1.9449)			2.047 (2.4683)	2.2363 (2.4704)	
30.0		1.85015 (1.852)	1.9041 (2.0725)	1.6162 (1.7215)		2.1249 (2.1623)	2.6001 (2.6447)	1.6989 (1.7295)
0.0	1.9891 (2.9076)	2.0925 (2.7092)	2.05 (2.5436)		2.2501 (3.2358)	2.3615 (3.1065)	2.3685 (2.1999)	
15.0		2.6333 (3.0212)	2.2001 (2.5171)			2.7919 (3.1989)	2.0785 (2.3955)	
30.0			2.6931 (2.7466)	1.852 (1.9469)			2.259 (2.3803)	1.855 (1.8834)

* In the direction perpendicular to the fitting plane.
+ In direction of the laser beam.

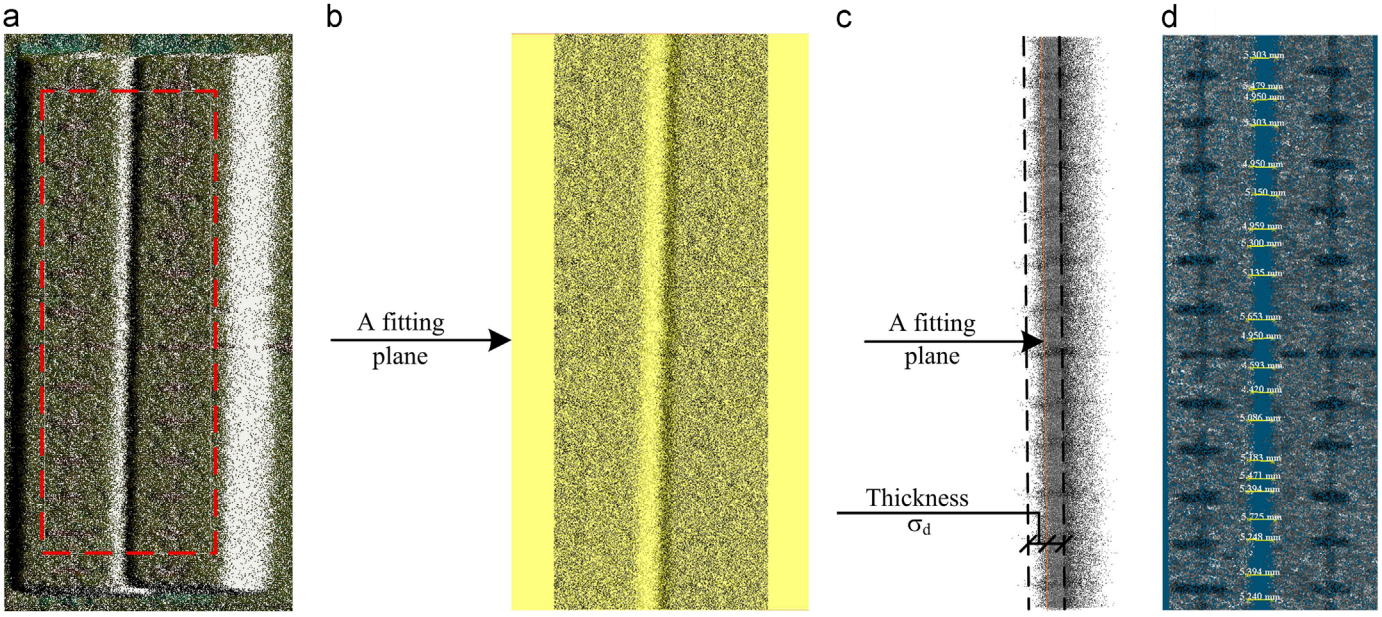

Fig. 7. Post-processing of point clouds to measure crack width. (a) 3D point cloud. (b) A fitting plane of data points of a sample's surfaces. (c) Extract data point of a sample's surface (side view). (d) Crack width measurements.

were not part of the sample's original surface. Then, a fitting plane was applied to generate a surface of the sample based on the remaining points (Fig. 7b). In actuality, the point cloud's surface was not lying within the same plane. This can be seen through the presence of noise (see Table 3). Therefore, the data points within a thickness, σ_d, from the fitting plane were chosen as the data points of the sample's surface for subsequent crack measurement, where σ_d is the perpendicular noise level of the range measurement (Fig. 7c). Finally, a built-in measurement tool in RWS V6.3 was used to measure the crack width, as the distance between two points belonging to the two edges of the gap (Fig. 7d). A pair of sample points on a cross-section of the crack along the vertical direction was randomly chosen to measure the crack width. This was done at approximately 5 mm intervals (Fig. 7d). The crack widths with the confidence level of 90% are shown in Table 4. Details of the procedure of computing the crack confidence limit are described in detail in Truong-Hong and Laefer [35]. Notably, the crack was not visible for the samples S1 and S2 at several scan locations (Table 4).

Eq. (5) implies that the crack depth is dependent upon three things: the orthogonal scan distance, the scan angle, and the crack width. Since fully opened cracks were used in the experiments, the laser beam's return at a scan angle of 0° was from the back of the crack (25 mm deep), but at other angles was returned from the side face of the crack. Under these conditions, the crack depth is determined by using Eq. (6). Results are as shown in Table 5.

Fig. 8 shows the predicted range of minimum, detectable crack widths according to Eq. (5) using the visible sides of the cracks' depths as shown in Table 5 at orthogonal scan distances of 5.0 m and 12.5 m. Incorporating the crack width-based TLS data into Fig. 8 explicitly shows that the width of all tested cracks detected fell within the detectable region, as determined by the theoretical, minimum, crack width curve corresponding to the appropriate crack depth. As such, at a scan angle of 0°, all tested cracks were in the detectable region (Fig. 8). Fig. 8 shows the region of 1–5 mm in which brick masonry is generally considered as "slightly" damaged [1].

When the orthogonal scan distances were obtained within 7.5 m of the target, the experimental results differed only slightly from the theoretical widths (Fig. 9). Beyond 7.5 m, larger errors were generated because of positional uncertainties that arose during scanning with large measurement ranges, namely the horizontal sampling step and the laser beam diameter increased [23]. The smallest relative difference was 0.13 mm ($D=5.0$ m, $\theta=0°$: 1.40 mm-theory vs. 1.53 mm-lab) for sample S1. The largest relative differences occurred when the scanner was further than 12.5 m from the sample. In general, differences occurred

Table 4
Confidence limits of crack width based TLS data with confidence level of 90%*.

θ (°)	D=5.0 m				D=7.5 m			
	S1 w=1.10	S2 w=3.14	S3 w=5.33	S4 w=7.22	S1 w=1.10	S2 w=3.14	S3 w=5.33	S4 w=7.22
0	1.53 ± 0.06	3.95 ± 0.08	5.35 ± 0.11	ND	2.26 ± 0.08	4.36 ± 0.14	5.97 ± 0.05	ND
15	NV	3.96 ± 0.14	5.43 ± 0.09	ND	NV	4.40 ± 0.11	6.19 ± 0.12	ND
30	NV	4.16 ± 0.14	5.43 ± 0.19	7.58 ± 0.15	NV	4.51 ± 0.17	6.58 ± 0.16	7.89 ± 0.16
θ (°)	D=10.0 m				D=12.5 m			
	S1 w=1.10	S2 w=3.14	S3 w=5.33	S4 w=7.22	S1 w=1.10	S2 w=3.14	S3 w=5.33	S4 w=7.22
0	2.72 ± 0.23	6.12 ± 0.10	8.41 ± 0.07	ND	5.91 ± 0.20	9.16 ± 0.11	11.08 ± 0.11	ND
15	NV	6.28 ± 0.18	8.46 ± 0.21	ND	NV	9.47 ± 0.27	11.3 ± 0.30	ND
30	NV	NV	9.13 ± 0.31	8.68 ± 0.28	NV	NV	12.02 ± 0.56	12.01 ± 0.46

* NV=non-visible; ND=no data collected at this location. At a 5 m offset at as little as 15°, 1 mm cracks stop being visible. At 30°, this happens with the 3 mm crack at 10 m and beyond.

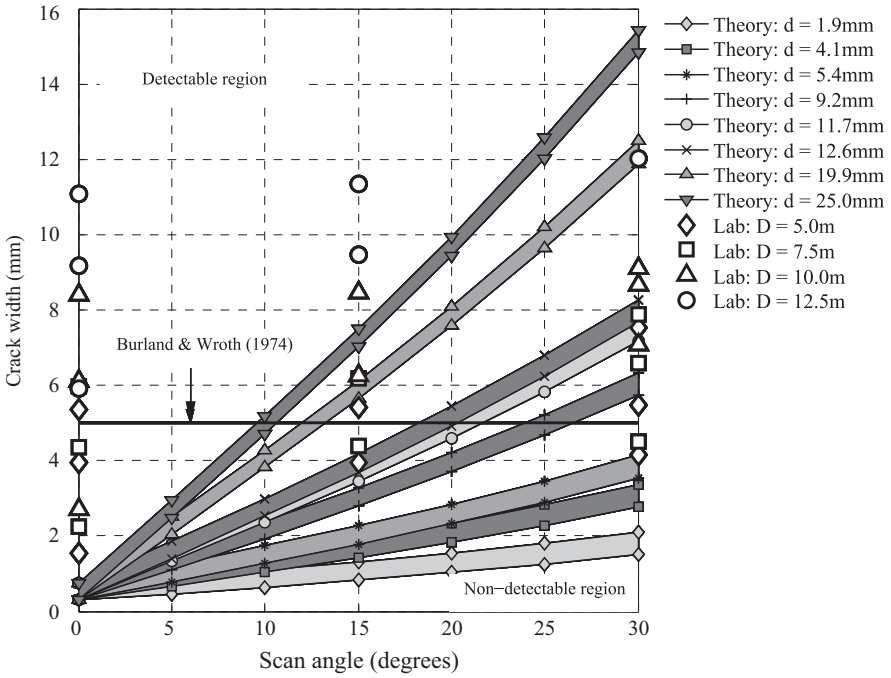

Fig. 8. Minimum visible crack width vs. scan angle at various crack depths overlaid with experimentally visible data.

because (1) the actual scan mechanism differs from theory because of positional uncertainty as described above, and erroneous measurement of the boundary due to occlusion [36]; (2) noise in the data (shown in Table 3) and (3) the fact that users cannot fully determine the exact points of the crack's edges because of the discrete nature of the data collection.

Experimental results indicate that crack widths appear larger at greater orthogonal distances and at larger scan angles, both of which were predicted. By comparing results of crack width-based TLS data to actual ones obtained from a mechanical probe, the minimum absolute errors of the crack width were shown to be 0.43 mm (D=5.0 m, θ=0°), 0.81 mm (D=5.0 m, θ=0°), 0.02 mm (D=5.0 m, θ=0°) and 0.31 mm (D=5.0 m, θ=30°) for samples S1–S4, respectively (Table 4). The maximum absolute errors were less than 1.16 mm and 1.37 mm for the orthogonal scan distances of 5.0 and 7.5 m, respectively. The orthogonal scan distance generated larger errors than changes in the scan angle. For example, for the sample S3 (w=5.33 mm), absolute errors of crack widths increased from 0.02 mm (5.35 mm vs. 5.33 mm) to 5.75 mm (11.08 mm vs. 5.33 mm) when the corresponding orthogonal distance (D) grew from 5.0 m to 12.5 m at a scan angle 0° (Table 4). For larger scan angles, the absolute errors increased only slightly. For example, at an orthogonal distance of 7.5 m, the crack width errors for sample S3 (w=5.33 mm) were respectively, 0.64 mm (5.97 mm vs.

Table 5
Theoretical crack depth subjected to various scan angle and predefined crack widths (mm).

θ (°)	S1 w=1.10 (mm)	S2 w=3.14 (mm)	S3 w=5.33 (mm)	S4 w=7.22 (mm)
15	4.1	11.7	19.9	27.1*
30	1.9	5.4	9.2	12.6

* In this case, since the laser beams hit and return from the wooden mounting board where the same was affixed, the crack depth equals the sample depth of 25 mm, instead of the theoretical value of 27.1 mm.

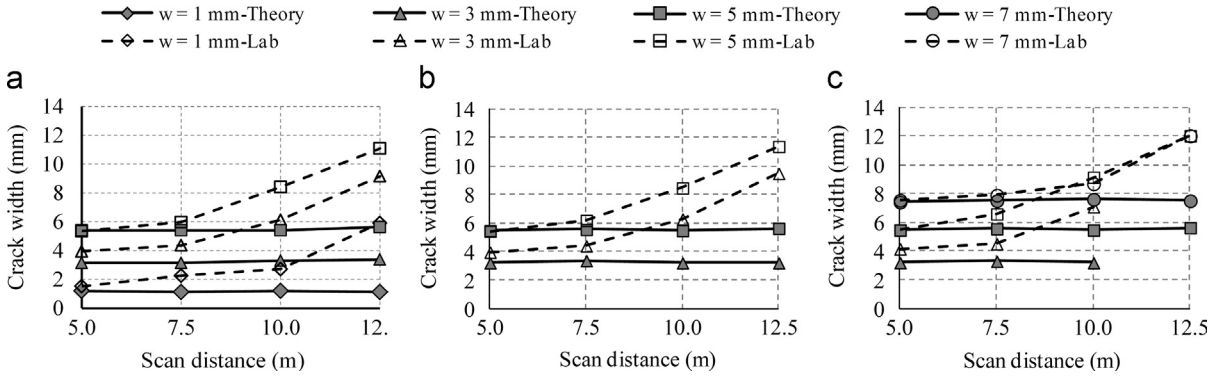

Fig. 9. Crack width predicted versus measured. (a) Scan angle at 0°, (b) Scan angle at 15° and (c) Scan angle at 30°.

5.33 mm), 0.86 mm (6.19 mm vs. 5.33 mm) and 1.25 mm (6.58 mm vs. 5.33 mm) at the scan angles 0°, 15°, and 30°.

6. Discussion

At a range of less than 10.0 m, TLS can reliably detect vertical cracks of at least 5 mm. This matches other experimental work proposing that a TLS unit performs reasonably well in the range of 6–12 m [37]. At the closest tested position ($D=5.0$ m, $\theta=0°$), the minimum absolute error was 0.02 mm for a 5.33 mm wide crack. The general trend was to overestimate the crack width. In a field study of two to four storey brick and rendered structures, Laefer et al. [37] found that the same TLS unit set 20–35 m away from the structures tended to overestimate crack widths by 7 mm with a 5 mm × 5 mm scan density. The acceptability of such deviations will depend upon the particular application.

In practice, the smallest crack width to be detected is dominated by two practical aspects involving the minimum sampling step and the footprint of the laser beam. With a specific distance, the overlapping laser spots can occur when the laser beam's footprint is enlarged greater than the sampling step. In this case, the full benefit of the correlated sampling is not realized [23]. In this study, a minimum visible crack width must be equal or greater than double the minimum sampling step. This assumption is sufficient to distinguish data points belonging to two different edges of the crack, although the measured points may be biased by up to one-half of the beam width [23]. This point is supported by previous work by Laefer et al. [31] that showed that the beam width accurately presents the scan resolution, if the sampling step is about 55% of the beam width. This condition can be set during data collection for crack detection. Therefore, the minimum crack width detected depends on a technical specification of the scanner and a scan distance, which controls the minimum sampling step and beam width. For example, when using the Trimble scanner GS200 to detect a 5 mm wide crack, the maximum distance from the scanner to the crack is theoretically around 80 m. This arrangement would allow the collected point cloud to satisfy the two constraining parameters (minimum sampling step and beam width).

As noted experimentally elsewhere [23,31,32], the orthogonal distance was more influential than the scan angle in controlling accuracy, even though the scan angle distorts the laser beam's footprint. Thus, a sampling step as a function of the scanner's distance from the target is the most important factor in TLS crack detection. As such, for the Trimble GS200, the sampling step increased from 0.15 mm to 0.38 mm when the range lengthened from 5.0 m to 12.5 m, while the footprint of the laser beam changed from $a/b=1.0$ ($\theta=0°$) to $a/b=1.167$ ($\theta=30°$), in which a and b are, respectively, the major and minor axes of the footprint of the laser beam [31].

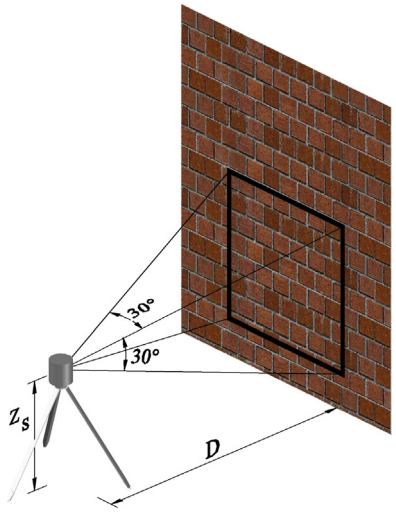

Fig. 10. Diagram to determine the best place of the crack.

In this study, the crack width-based TLS data were manually measured by using RWS V6.3 [34] associated with the Trimble GS200. As noise in the data occurs, manually determining the crack edges is still challenging. Selected point clouds may belong to either the sample surface or a crack side perpendicular to the sample surface. In addition, the incidence angle may affect the quality of the point clouds, in which uncertainty may occur [32] especially when the off-set distance exceeds 7.5 m. Therefore, an automatic method to determine crack width from TLS data to eliminate user errors would be highly useful.

For best results the scanner should be set at an orthogonal distance of no more than 7.5 m and within a scan angle of 15°. This implies the best place for crack detection is within a back clipping plane of a frustum view, where a field of view angle is 30°, and the viewing direction is along a horizontal direction (Fig. 10). For example, if the scanner is 5.0 m away from the building and mounted 2.0 m above the ground level, the back clipping plane is defined by a pair of coordinates ($x \in [-1.34$ m, 1.34 m], $y \in [0.66$ m, 3.34 m], where the projected scanner mount on the vertical wall has an x-coordinate of 0.0 m and a y-coordinate of 2.0 m. In urban areas with narrow footpaths, such locations may impede street usage. Finally, the accuracy of the crack width can be obviously improved when a scan unit with a higher sampling step and high accuracy of point measurement is used.

Clearly, crack width-based TLS data in this study are less accurate than that obtained from manual measurement and digital image-based on edge detection techniques, which have been

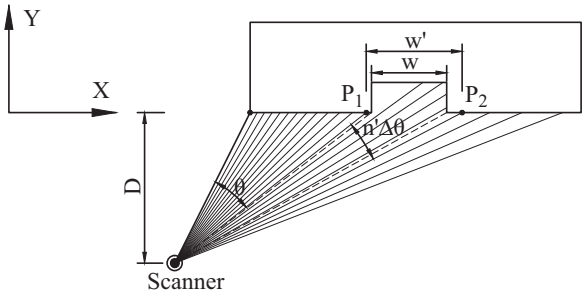

Fig. 11. Practically determining crack width by TLS.

shown to be respectively ±1 mm and at least 1 pixel [13,17]. However, TLS usage circumvents scaffold usage [37] and the need to know a camera's focal length and distance to the target surface [13]. Additionally there are issues of speed and permanency. Herein, each position of each sample took approximately 2.5 min for scanning and another 3 min for post-processing crack measurement. In a field study, Laefer et al. [37] concluded that using TLS generated more consistent, as well as more cost efficient detection than manual techniques. Similarly, Olsen et al. [6] found that TLS compared favourably to conventional photography under laboratory conditions.

7. Conclusions

This paper confirmed in broad terms masonry crack detection limits of a proposed set of fundamental mathematics. In addition, laboratory tests showed that errors of the crack width-based TLS data were small when the orthogonal distances from the scanner to the samples were varied from 5.0 to 7.5 m but significantly increased for more distant scanner locations. At an orthogonal distance of 5.0 m, the maximum absolute errors were respectively, 1.16 mm and 0.10 mm for the samples having predesigned crack widths of 1–3 mm and 5 mm. Based on these results, it is arguably concluded that TLS can consistently acquire data points for detecting cracks in masonry structures crack widths greater than 5 mm. With the tested equipment at an orthogonal distance of 5 m and a scan angle of 0°, the absolute error was only 0.015 mm. While, the scan angle may restrict crack detection because of the visibility of noise on the crack's edge, the orthogonal distance is more influential in controlling the accuracy. As the laboratory tests herein were only for vertical cracks, additional experimental work is needed for development of diagonal crack limits, but arguably more importantly, an automatic approach to identify cracks within TLS data must be developed to overcome user-based detection errors.

Acknowledgments

Support for this work was generously provided by Science Foundation Ireland, Grant 05/PICA/I830 and by the European Union's ERC-2012-StG_20111012 Project 307836.

Appendix A. Error propagation of the crack width-based TLS data

Eq. (12) was established to calculate the theoretical crack width based on point cloud, which is to compute a distance between two corners of a crack. By substituting number of angular steps (n') calculating from Eq. (13) into Eq. (12), this equation can be rewritten as:

$$w' = D\ \tan(\theta + n'\Delta\theta) - D\ \tan\ \theta \tag{17}$$

where D tan $(\theta+n'\Delta\theta)$ and D tan θ are respectively standing for x_2 and x_1 coordinates of the point P_1 and P_2 (Fig. 11).

Eq. (17) is now rewritten as:

$$w' = x_2 - x_1 \tag{18}$$

Eq. (18) implicitly imposed that the crack width is determined from the coordinates of the point clouds belonging to the two opposite faces of the crack, which is shown in Eq. (17). Therefore, an error of crack width depends on the errors of the acquired point clouds, (P_1 and P_2).

By applying the addition rule of error propagation, the uncertainty of Eq. (18) in quadrature is presented:

$$\delta_{w'} = \sqrt{(\delta_{x_1})^2 + (\delta_{x_2})^2} \tag{19}$$

where δ_{x1} and δ_{x2} are errors of acquired data points P_1 and P_2, respectively. In addition, the error of point cloud acquisition of TLS can be expressed as proposed by Cuartero et al. [38]:

$$\delta_p = \sqrt{(\delta_x)^2 + (\delta_y)^2 + (\delta_z)^2} \tag{20}$$

where δ_x, δ_y and δ_z are errors of the point in each axis X, Y, and Z in Cartesian coordinate. Roughly assuming that the error occurs simultaneous in all three directions, Eq. (20) can be rewritten:

$$\delta_p = \sqrt{3}\ \delta_x \tag{21}$$

Similarly with equal errors of data points P_1 and P_2 in the X direction and substituting Eq. (21) into Eq. (19), the error of the theoretical crack width is expressed as:

$$\delta_{w'} = 0.816\delta_p \tag{22}$$

As part of the equipment specifications of the Trimble scanner GS 200 the error in point position by 1.4 mm for a range of 5–50 m, the error of the theoretical crack width is 1.22 mm.

References

[1] Burland JB, Wroth CP. Settlement of buildings and associated damage. In: The British geotechnical society's conference on the settlement of structures. Cambridge. 1974: 611-54.
[2] Chung HW. Assessment and classification of damages in reinforced concrete structures. Concr Int 1994;16:55–9.
[3] Marazzi F, Tagliabue P, Corbani FM. Traditional vs innovative structural health monitoring of monumental structures: a case study. Struct Contr Health Monit 2011;18:430–49.
[4] Ritdumrongkul S, Fujino Y. Identification of the location and size of cracks in beams by a piezoceramic actuator–sensor. Struct Contr Health Monit 2007;14:931–43.
[5] Laflamme S, Kollosche M, Connor JJ, Kofod G. Soft capacitive sensor for structural health monitoring of large-scale systems. Struct Contr Health Monit 2012;19:70–81.
[6] Olsen MJ, Kuester F, Chang BJ, Hutchinson TC. Terrestrial laser scanning-based structural damage assessment. J Comput Civil Eng 2010;24:264–72.
[7] Monserrat O, Crosetto M. Deformation measurement using terrestrial laser scanning data and least squares 3d surface matching. ISPRS J Photogramm Remote Sens 2008;63:142–54.
[8] Gordon SJ, Lichti DD, Franke J, Stewart MP. Measurement of structural deformation using terrestrial laser scanners. In: First FIG international symposium on engineering surveys for construction works and structural engineering. Nottingham, United Kingdom; 2004. 16.
[9] Armesto-González J, Riveiro-Rodríguez B, González-Aguilera D, Rivas-Brea MT. Terrestrial laser scanning intensity data applied to damage detection for historical buildings. J. Archaeol. Sci. 2010;37:3037–47.
[10] Teza G, Galgaro A, Moro F. Contactless recognition of concrete surface damage from laser scanning and curvature computation. NDT and E Int 2009;42:240–9.
[11] Soldovieri F, Dumoulin J, Masini N, Utsi E. Noninvasive sensing techniques and geophysical methods for cultural heritage and civil infrastructures monitoring. Int J Geophy 2011;2011:1–2.

[12] Colombo IS, Main IG, Forde MC. Assessing damage of reinforced concrete beam using "b-value" analysis of acoustic emission signals. J Mater Civ Eng 2003;15:280–6.
[13] Barazzetti L, Scaioni M. Crack measurement: development, testing and applications of an automatic image-based algorithm. ISPRS J Photogramm Remote Sens 2009;64:285–96.
[14] Hampel U, Maas HG. Cascaded image analysis for dynamic crack detection in material testing. ISPRS J Photogramm Remote Sens 2009;64:345–50.
[15] Niemeier W, Riedel B, Fraser C, Neuss H, Stratmann R, Ziem E. New digital crack monitoring system for measuring and documentation of width of cracks in concrete structures. In: Thirteenth FIG symposium on deformation measurement and analysis, 14th IAG symposium on geodesy for geotechnical and structural engineering. Lnec, Lisbon; 2008. 9.
[16] Dare P, Hanley H, Fraser C, Riedel B, Niemeier W. An operational application of automatic feature extraction: the measurement of cracks in concrete structures. Photogramm Rec 2002;17:453–64.
[17] Sohn H-G, Lim Y-M, Yun K-H, Kim G-H. Monitoring crack changes in concrete structures. Comput -Aided Civ Infrastruct Eng 2005;20:52–61.
[18] Habib A, Kelley D. Single-photo resection using the modified hough transform. Photogramm Eng Remote Sens 2001;67:909–14.
[19] Al-Neshawy F, Piironen J, Peltola S, Erving A, Heiska N, Nuikka M, et al. Measuring the bowing of marble panels in building facades using terrestrial laser scanning technology. J Inf Technol Constr 2010;15:64–74.
[20] Girardeau-Montauta D, Roux M, Marc R, Thibault G. Change detection on points cloud data acquired with a ground laser scanner. ISPRS WG III/3, III/4, V/3 workshop Laser Scanning 2005. Enschede, The Netherlands, 2005: 30-5.
[21] Liu W, Chen S, Hauser E. Lidar-based bridge structure defect detection. Exp Tech 2011;35:27–34.
[22] Tsai Y-CJ, Li G. Critical assessment of detecting asphalt pavement cracks under different lighting and low intensity contrast conditions using emerging 3d laser technology. J Transp Eng 2012;138:649–56.
[23] Lichti DD, Jamtsho S. Angular resolution of terrestrial laser scanners. Photogramm Rec 2006;21:141–60.
[24] Pesci A, Teza G, Bonali E. Terrestrial laser scanner resolution: numerical simulations and experiments on spatial sampling optimization. Remote Sens 2011;3:167–84.
[25] DeltaSphere Inc. Deltasphere-3000ir 3d laser scanner and scene digitizer. 2011; Accessed date: 15 October, 2012. ⟨http://www.deltasphere.com/deltasphere3000_specs.htm⟩.
[26] FARO Technologies Inc. Faro laser scanner focus3d. 2011; Accessed date: 15 October, 2012. ⟨http://www.faro.com/focus/us⟩.
[27] Trimble Navigation Limited. Trimble fx 3d scanner. 2012; Accessed date: 15 October, 2012. ⟨http://www.trimble.com/power-process-plant/Trimble-FX-3D-Scanner.aspx⟩.
[28] Optech Incorporated. Ilris laser scanner. 2009; Accessed date: October 15, 2012. ⟨http://www.optech.ca/pdf/Brochures/ILRIS-DS-LR.pdf⟩.
[29] Leica Geosystems. Leica scanstation c10. 2012; Accessed date: 15 October, 2012. ⟨http://hds.leica-geosystems.com/en/Leica-ScanStation-C10_79411.htm⟩.
[30] RIEGL Laser Measurement Systems. Riegl vz-6000. 2011; Accessed date: 15 October, 2012. ⟨http://www.riegl.com/uploads/tx_pxpriegldownloads/DataSheet_VZ-6000_24-09-2012.pdf⟩.
[31] Laefer DF, Fitzgerald M, Maloney EM, Coyne D, Lennon D, Morrish SW. Lateral image degradation in terrestrial laser scanning. Struct Eng Int 2009;19:184–9.
[32] Soudarissanane S, Lindenbergh R, Menenti M, Teunissen P. Incidence angle influence on the quality of terrestrial laser scanning points Laserscanning '09. Paris, France; 2009; XXXVIII:183–8.
[33] Trimble. Gs200 3d scanner. 2003; Accessed date: July 30, 2013. ⟨http://www.trimble.com/gs200.shtml⟩.
[34] Trimble Navigation Limited. Realwork survey advanced v6.3. 2005; Accessed date: October 15, 2012. ⟨http://www.trimble.com⟩.
[35] Truong-Hong L, Laefer DF. Validating computational models from laser scanning data for historic facades. J Test Eval 2013;41:16.
[36] Sotoodeh S. Outlier detection in laser scanner point clouds. ISPRS Commission V Symposium: Image Engineering and Vision Metrology. Dresden, Germany; 2006; XXXVI:297–302.
[37] Laefer DF, Gannon J, Deely E. Reliability of crack detection methods for baseline condition assessments. J Infrastruct Syst 2010;16:129–37.
[38] Cuartero A, Armesto J, Rodriguez PG, Arias P. Error analysis of terrestrial laser scanning data by means of spherical statistics and 3d graphs. Sensors 2010;10:10128–45.